PHYSICAL REVIEW B VOLUME 25, NUMBER 3 1 FEBRUARY 1982

Neutron scattering study of the tetragonal-to-incommensurate ferroelastic transition in barium sodium niobate

J. Schneck and J. C. Tolédano
Centre National d'Etudes des Télécommunications, 92220 Bagneux, France

C. Joffrin*
Institut Laue Langevin, 156 X, 38042 Grenoble-Cédex, France

J. Aubree, B. Joukoff, and A. Gabelotaud
Centre National d'Etudes des Télécommunications, 92220 Bagneux, France
(Received 10 August 1981)

The static and dynamic characteristics of the incommensurate phases of barium sodium niobate have been investigated by means of elastic and inelastic neutron scattering between room temperature and 660 °C. The observation of two incommensurate phases on heating from room temperature is consistent with previous x-ray results. Phase II, which is stable up to $T_{II}=250$ °C, is nearly commensurate, the modulation vector being $\vec{k}=[(\vec{a}^*+\vec{b}^*)(1+\delta)/4+\vec{c}^*/2]$, with $\delta\approx 1\%$. Phase I is incommensurate with the same direction of modulation, and δ varies linearly on heating from 8% at T_{II}, up to 12.5% at $T_I\simeq 288$ °C. Above T_I, crystalline phases with tetragonal symmetries are stable, T_{II} is discontinuous, and T_I continuous. On cooling down from T_I a large thermal hysteresis is noted in the modulation wavelength and the satellite intensities. The variations are smeared and no discontinuity similar to T_{II} is observed. The precursor effects of T_I consist, in the tetragonal phase, of a soft phonon and a central peak. The soft mode is underdamped only above ~385 °C. The static susceptibility deduced from the total scattered intensity diverges at T_I, with $\omega_0^2\sim 1/\chi$, varying linearly between 300 °C and 360 °C. The central peak, which is observed even at 660 °C, diverges at T_I while its width remains always equal to the instrumental width. The dispersion surface of the soft mode in the $(\eta\xi\frac{1}{2})$ plane has a valley shape, the bottom of which is perpendicular to the modulation vector. It gives rise to diffused scattering forming rods along $[1\bar{1}0]$. At a microscopic level the modulation is due to displacements consisting of a collective shearing of the oxygen octahedra in the structure. The dynamics of this motion involve strong correlations in planes containing the modulation vector and the polar c axis. The order parameter of the observed sequence of transitions has four components. This unusual dimension is responsible for the breaking of the macroscopic symmetry in the incommensurate phases and the onset of improper ferroelastic properties. However, the incommensurate behavior deriving from it is expected to be the same as that previously studied for two-component order parameters. Thus the corresponding extended Landau theory is not likely to account for the unusual hysteresis observed below T_I, and for the persistence of a residual incommensurability below T_{II}. These anomalous effects are attributed to the influence of defects having their origin in an off-stoichiometry or off-equilibrium distribution of the cations in the structure.

I. INTRODUCTION

A large number of mixed-oxide compositions, possessing ferroelectric properties, crystallize in the tetragonal tungsten bronze structure.[1] This structure owes its name to its close relationship with the structure of potassium tungsten bronze K_xWO_3.[2] It consists of a skeleton of oxygen octahedra sharing corners and forming various types of tunnels, running along the c direction, in which cations are located.[1] An approximate symmetry of all the members of the structural family is represented by

the tetragonal space group $P4/mbm(D_{4h}^5)$ with parameters $a_t \simeq 12.4$ Å and $c_t \simeq 4$ Å (i.e., the height of one oxygen octahedron). In most substances, the phase observed at room temperature has a structure which is slightly distorted with respect to the reference structure. It has a polar tetragonal or orthorhombic symmetry.[1]

Some of the tungsten bronze ferroelectrics, namely lead metaniobate,[3] and the alkali-alkaline earth niobates[4] have been the subjects of intensive investigations. This interest has been motivated by actual or potential applications of these materials based on their outstanding piezoelectric, electro-optical, and nonlinear optical responses.[5] Most of the studies were, however, restricted to the evaluation and optimization of these useful properties. Less attention has been given to the characterization and understanding of their structural phase transitions. In particular, for the alkali-alkaline earth niobates the crystallographical description of the different phases is still incompletely known. Likewise, physical measurements across the phase transitions are scarce.

Barium sodium niobate, $Ba_2NaNb_5O_{15}$ (BSN), is, at present, the best characterized of these compounds, though many of its features are still not clearly understood. An intricate pattern of phase transitions has been observed in this compound. A standard ferroelectric transition ($4/mmm \rightarrow 4mm$) accompanied by a divergence of the dielectric susceptibility along $\vec{c}$ occurs at about 580 °C.[6] At lower temperatures, BSN undergoes at least two structural transformations. The first, near 300 °C, corresponds to the onset of an orthorhombic phase[4] ($mm2$) which remains stable down to -160 °C. Below this temperature a tetragonal symmetry is recovered.[7] Additional anomalies whose possible relationships with phase transitions have not yet been demonstrated were also detected in the temperature dependences of the optical birefringence and the shear strain in the *ab* plane (-100 °C) as well as in the dielectric permittivity in the same plane (-260 °C).[8] On the other hand, an incipient structural instability has been revealed by the softening of an underdamped optic mode whose squared frequency decreases linearly on cooling down to 1.5 K.[9] It has been noted[10] that some of the preceding features were very sensitive to a deviation from the stoichiometric composition, while others were relatively independent of compositional changes. Finally, the existence of incommensurate phases in BSN has recently been postulated[11] and subsequently confirmed.[12]

The 300 °C phase change from a tetragonal to an orthorhombic symmetry has been the focus of most of the experimental and theoretical efforts in the past years. This change involves a small shearing ($\simeq 6'$ at room temperature) of the tetragonal unit cell in the *ab* plane. It gives rise to ferroelastic domains[4] characterized by opposite values of the shear.

Three stages can be distinguished in the progressive clarification of the mechanism of this transition, due to improved accuracy and completeness of the available experimental data.

In the first place, noting the occurrence of a softening in the orthorhombic elastic constants C_{11} and C_{22} at 300 °C, Yamada[13] assumed that the transition was driven by an elastic instability of the lattice, and thus developed a phenomenological model in which the order parameter coincided with the shear strain e_{ab}. In this approach, the transition was expected to preserve the translational periodicity of the crystal ($\vec{k}=0$).

One of us pointed out[14] that the preceding interpretation was incompatible with the temperature dependence of the elastic anisotropy ($C_{22}-C_{11}$) which was obtained from Brillouin scattering measurements.[15] The onset of the shear strain e_{ab} was suggested to be a secondary effect of the transition, resulting from a quadratic coupling of e_{ab} to another degree of freedom, constituting the true order parameter of the transition. By taking into consideration the room-temperature structural data of Jamieson *et al.*[16] and the superlattice periodicity along the *c* axis subsequently discovered,[4,17] this order parameter was inferred to be a "zone-boundary" degree of freedom whose onset should induce a breakdown of the translational periodicity along the *c* direction ($\vec{k}=\vec{c}^{\,*}/2$). An experimental confirmation of this translational change was brought by Burgeat *et al.*,[18] who demonstrated, through x-ray rotation photographs along $\vec{c}$, the vanishing of the $c^*/2$ superlattice layer lines above $T_I \simeq 300$ °C. Consistently, Raman scattering measurements by Boudou *et al.*[19] disclosed additional lines in the spectra below T_I, denoting the multiplication of the number of atoms in the unit cell.

Recently, an x-ray Buerger precession experiment[12] has shown that there were actually two transitions in the 300 °C range, separated by ~ 30 °C. The upper transition near 300 °C corresponds to the onset of a phase which has, in addition to the previously established superlattice period along $\vec{c}$, an incommensurate modulation along the [110] tetragonal direction. The ortho-

rhombic symmetry previously observed is only that of the "average" crystalline structure. The lower transition leads to another incommensurate phase with identical point symmetry and the same direction of modulation but with a different periodicity very close to a commensurate one. This phase is stable at room temperature. Above 300 °C precursor effects of the tetragonal-orthorhombic transition were observed under the form of diffused rods joining the satellites along the $[1\bar{1}0]$ direction.

These results needed a quantitative confirmation and completion. In particular, the temperature dependence of the modulation and of the satellite's intensity was not accurately specified by the x-ray technique. On the other hand, it provided no insight on the dynamical instabilities related to the phase transitions and left unexplained the origin of the observed diffused scattering.

In order to clarify these points we have undertaken an investigation of BSN by means of the elastic and inelastic scattering of thermal neutrons, which is presented in the following sections. Section II specifies the experimental conditions of the investigation. Section III contains the results of the measurements as well as the derivation of the relevant characteristics of the transitions considered: static behavior in the incommensurate phases and dynamical properties on approaching the tetragonal-incommensurate transition. Section IV is devoted to the discussion of these results with respect to the previously known experimental data for BSN as well as to the standard behavior expected for incommensurate substances. In particular, the symmetry properties and the microscopic nature of the order parameter are specified. Important qualitative deviations from the standard behavior of incommensurate systems are pointed out.

II. EXPERIMENTAL PROCEDURE

Two experiments were performed for the purpose of exploring two different scattering planes. The two crystals used were grown in our laboratory (CNET) by the Czochralski pulling procedure previously described.[10] Their volumes were approximately 4 cm^3 ($\sim$20 g). Though the starting melt had the stoichiometric composition, the resulting crystals were slightly enriched in barium content, consistent with the segregation trend well established for this substance.[10,16,20] For instance, the formulas determined for one of the samples by a radioactivation method[10] were $Ba_{2.08}Na_{0.84}Nb_5O_{15}$ for the head of this large rod and $Ba_{2.06}Na_{0.88}Nb_5O_{15}$ for its tail.

The samples were handled as grown with only a rough polishing of the faces perpendicular to the c direction. This operation was performed in order to allow a preorientation in the neutron beam, based on visually locating the directions of the ferroelastic domain walls. The crystals were not detwinned either electrically or mechanically. Accordingly, in addition to the ferroelastic domains which are easily detected visually, they were expected to possess ferroelectric domains which arise from the 580 °C transition and coexist with the ferroelastic ones at room temperature.

The ferroelectric twinning, which reverses the polarity of the c axis, was not likely to influence the observations relative to the considered transition. In contrast, the ferroelastic twinning could perturb the measurements, as it interchanges the a and b directions and mixes (hkl) reflections with (khl) reflections. In particular, it could give the appearance of a modulation along both orthorhombic axes while actually a modulation along only one axis exists.[12]

It is, however, our previous experience that as-grown samples of BSN will always display a largely predominant ferroelastic orientation, with the perpendicular orientation only realized in small regions spread, more or less uniformly, in the volume of the sample. Moreover, this domain configuration will change very little with variation of temperature, and will reorient with the same pattern after each crossing of the tetragonal-orthorhombic transition. In this respect BSN differs from most other ferroelastic materials, such as gadolinium molybdate in which the domain pattern undergoes major modifications on approaching the transition or on heating and then cooling through it. This is a fortunate circumstance, not yet well understood, because once the crystal has been set to the predominant orientation, its setting will be preserved throughout the experiment. This setting was achieved by resolving the high-order reflections (1200) and (0120) relative to the pseudocrystalline orthorhombic subcell, and taking into account the slightly different values of its parameters, $a_0 \simeq 17.59$ Å and $b_0 \simeq 17.62$ Å. In this way, the scattering plane was fixed to contain the a orthorhombic axis for the predominant domain orientation.

Above 300 °C, the tetragonal phase possesses a

simple tetragonal Bravais lattice[12] with $a_t = b_t \simeq 12.4$ Å and $c_t \simeq 4$ Å. With respect to the tetragonal translations the orthorhombic translations $\vec{a}_0$ and $\vec{b}_0$ are rotated by 45° around the common c axis. Throughout the following discussion, unless stated otherwise, the labeling of the orientations and of the reflections will be referred to the tetragonal system of axes both in direct and reciprocal space.

The two scattering planes investigated [Fig. 1(a)] were the $(1\bar{1}0)$ plane (containing the modulation vector) and the (100) plane. The first was used to obtain the characteristics of the modulation as well as the dynamics of the 300 °C transition at the critical wave vector and along the modulation direction. The second plane has allowed an investigation of the diffused scattering in the perpendicular direction.

The elastic and inelastic neutron scattering measurements were performed on the triple-axis spectrometer IN2 at the Laue Langevin Institute. This spectrometer uses pyrolytic graphite crystals as the monochromator and analyzer. The incident energy of the beam was kept constant during the scans at 13.5 meV (2.662 $Å^{-1}$). This wavelength

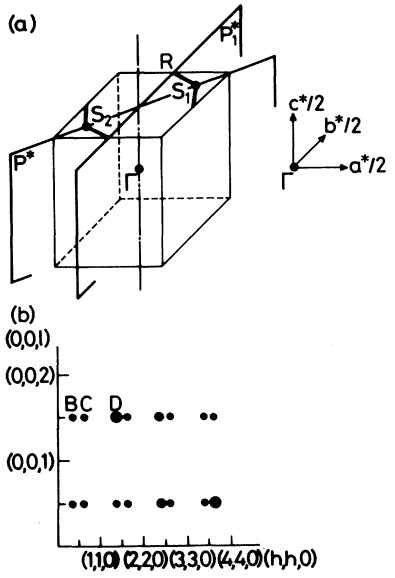

FIG. 1. (a) Reciprocal lattice of the high-temperature phase. P^* and P_1^* are the scattering planes explored in the experiment. S_1 and S_2 correspond to the satellites which appear in the incommensurate phase at $\vec{k} = \pm [1 + \delta)(a_t^* + b_t^*)/4 + c_t^*/2]$. The solid lines represent rods of diffuse scattering. (b) Distribution of the satellites intensities in the scattering plane P^*.

allowed an exploration of a region in reciprocal space extending approximately to the $(\frac{13}{2}\ \frac{13}{2}\ 0)$ reflection in the ab plane and to the $(0\,0\,\frac{7}{2})$ reflection in the c direction. The accessible energy transfer range was 0—1.5 THz. Contamination of the incident beam by harmonics of the former wavelength could be removed by inserting, before the sample, an additional pyrolytic graphite filter. An upper limit of the energy resolution was ~0.15 THz (5 cm^{-1}). The results of the inelastic scans were corrected for the dependence of the reflectivity of the analyzer on the wavelength.

At each temperature, the two crystallographic parameters defining the positions of the Bragg reflections of the basic structure in the scattering plane were adjusted. This provided us, besides an accurate scaling of the Brillouin zone, with an approximate plot of the thermal expansion of BSN in the relevant crystallographic directions.

Heating of the samples, during the two experiments, was achieved between room temperature and 660 °C in vacuum cells by means of the thermal radiation of an electrically heated cylindrical foil of niobium surrounding the crystals. To limit the temperature gradient, the sample was wrapped in a thin niobium foil which also served to maintain it in a holder. The temperature stability achieved in the measurement range was ~1 °C. The temperature was probed by means of a chromel-alumel thermocouple situated at some distance of the sample. Consequently, its indications were expected to differ from the actual temperature of the crystal. They were only used to provide us with a relative temperature scale. The absolute scaling was realized by associating the transition temperatures located in the neutron experiment to their values in the same sample, obtained by other techniques. In this view, differential thermal analysis, birefringence, and dielectric measurements were performed subsequently to the neutron measurements. Also, the thermal expansion variations obtained from the parameter fitting were compared to the existing data.[20]

III. EXPERIMENTAL RESULTS

As shown by the existing x-ray data,[12] the reflections of BSN are located at

$$\vec{G} = h\vec{a}_t^* + k\vec{b}_t^* + l\vec{c}_t^* + m\vec{k}\ , \qquad (1)$$

where the modulation vector $\vec{k}$ is

$$\vec{k}=\frac{\vec{a}_t^*+\vec{b}_t^*}{4}(1+\delta)+\frac{\vec{c}_t^*}{2} . \quad (2)$$

It involves a doubling of the periodicity along $\vec{c}$ and a modulation along [110]. The value $m=0$ in Eq. (1) corresponds to the main Bragg reflections associated to the average crystalline structure. Above the tetragonal-orthorhombic transition T_I, these reflections form the entire Bragg spectrum of BSN.[12] They occupy the vertices of a simple tetragonal lattice. Below T_I, this lattice is slightly distorted into a one-face centered orthorhombic lattice. The average orthorhombic structure has the space group $Cmm2$.[16] The values $m\neq 0$ correspond to the satellite reflections, vanishing above T_I.

In the $(1\bar{1}0)$ scattering plane the main reflections are of the form (hhl), while the first-order satellites are located at

$$\left[h\pm\frac{1+\delta}{4}\ h\pm\frac{1+\delta}{4}\ \frac{2l+1}{2}\right] .$$

The distribution of elastic neutron intensities of the first-order satellites belonging to the accessible range of the scattering plane is schematically reproduced in Fig. 1(b). The two most intense satellites are

$$\left[1+\frac{1+\delta}{4}\ 1+\frac{1+\delta}{4}\ \frac{3}{2}\right]$$

and

$$\left[4-\frac{1+\delta}{4}\ 4-\frac{1+\delta}{4}\ \frac{1}{2}\right] .$$

A preliminary measurement at room temperature in both the $(1\bar{1}0)$ and (110) planes and a fit of the parameters have enabled us to verify that the satellites, which appear on one of the bisectors of the tetragonal cell[12] lie in the a orthorhombic direction (corresponding to the shorter axis in the ab plane).

A. Static behavior below T_I

In the elastic neutron scans, the value of δ can be deduced from the relative locations of three neighboring first-order satellites belonging to the same layer line $(2l+1)/2$. These three reflections correspond, for instance, to $(h;m=\pm 1)$ and $(h+1;m=-1)$. If B, C, and D label the three positions we have [Fig. 1(b)]

$$\delta=\frac{|CD-BC|}{CD+BC} . \quad (3)$$

This determination of δ has the advantage of being insensitive to an imperfect fitting of the a_t^* parameter, in contrast to the measurement of the absolute position of a single satellite referred to the origin.

Let us examine the static characteristics of the modulation on heating the crystal between the room temperature (RT) and the temperature T_I of restoration of the tetragonal crystalline phase. At RT, δ is very small.[12] In order to determine its value, three groups of three neighboring satellites located in the layer lines $\frac{1}{2}$, $\frac{3}{2}$, and $\frac{5}{2}$ were scanned in the [110] and [001] directions, after careful refinement of the reciprocal-lattice parameters. The resulting value was $\delta=0.012\pm 0.001$, corresponding to the modulation vector $\vec{k}=(0.253, 0.253, 0.500)$. The difference between this vector and $\vec{k}_0=(0.25,0.25,0.5)$, which would correspond to a commensurate superstructure, is much larger than the experimental uncertainty, thus confirming the incommensurate nature of the RT phase.

On heating the sample, the variations of δ and those of the width and intensity of the first satellites reveal the existence of three phases: phase II,

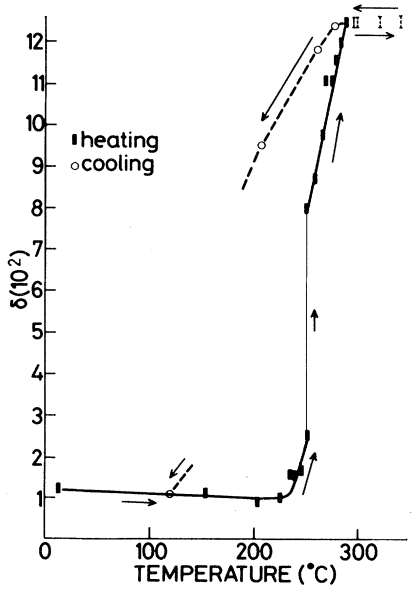

FIG. 2. Temperature dependence of the δ parameter characterizing the incommensurate modulation. Heating: filled squares. Cooling: open circles. Above ~ 288 °C the experimental points obtained on heating and on cooling coincide.

stable up to $T_{II} \approx 250\,^{\circ}C$, phase I, stable between T_{II} and $T_I \approx 288\,^{\circ}C$, and the tetragonal phase.

In phase II, δ is almost constant (Fig. 2) up to 230 °C, with a slight dip at about 200 °C. Above $\sim 230\,^{\circ}C$ a rapid increase takes place, reaching the value 0.025 ± 0.002 at 250 °C [$\vec{k} = (0.256, 0.256, 0.5)$]. In the whole range of temperatures below T_{II}, the width of the satellite remains equal to the instrumental width (Fig. 3), while its intensity drops by a factor of ~ 3 (Fig. 4). It has been pointed out[21] that the measured temperature dependence of the intensity could differ in a large sample from the actual dependence due to multiple scattering. This effect is expected to reduce the intensity of the strongest reflections. Thus it will be more sensitive in phase II, as well as for the most intense satellites. To remove this uncertainty we have compared the variations of the

$$\left[1+\frac{1+\delta}{4}\ 1+\frac{1+\delta}{4}\ \frac{3}{2}\right]$$

and

$$\left[2-\frac{1+\delta}{4}\ 2-\frac{1+\delta}{4}\ \frac{3}{2}\right]$$

satellites, whose intensities differ by an order of magnitude. The good agreement of their two temperature dependences suggests that the measured variations are intrinsic.

On setting the temperature $T_{II} = 250 \pm 2\,^{\circ}C$, a qualitatively different behavior is observed. On repeatedly scanning the satellite

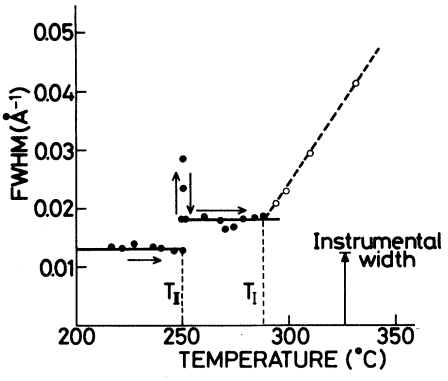

FIG. 3. Temperature variation of the full width at half-maximum (FWHM) of the incommensurate satellites. The open circles correspond to the diffused scattering above T_I. The experimental points at T_{II} are obtained during the occurrence of the first-order transition (see text).

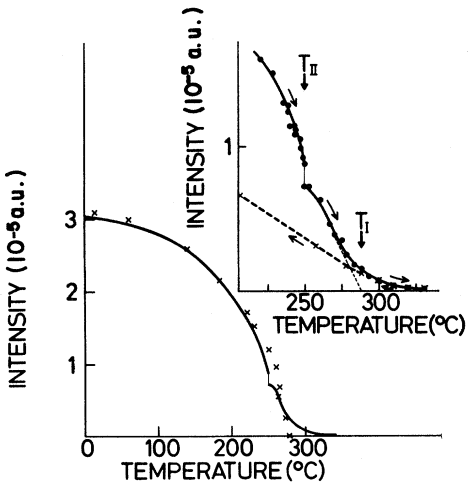

FIG. 4. Temperature dependence of the intensity of the incommensurate satellites (solid line). The crosses in the lower diagram represent properly scaled values of the spontaneous strain determined by γ-ray diffractometry. The inset is an expansion in the region of the transitions showing the thermal hysteresis.

$$\left[1+\frac{1+\delta}{4}\ 1+\frac{1+\delta}{4}\ \frac{3}{2}\right]$$

in the [110] direction, a slow evolution of the q spectrum occurs on a time scale which is much larger than that needed for the sample to reach its equilibrium temperature (Fig. 5). First, a main peak is recorded (curve 1), whose location, intensity, and width closely coincide with the characteristics of the satellite measured a few degrees Centigrade below T_{II}. In addition, the spectrum contains an asymetric tail in the q range corresponding to higher values of δ. The spectrum then evolves and consists of a much broader peak (up to 2.5 times the instrumental width) with a smaller intensity (curves 2 and 3). At some point two peaks can be distinguished in the broad feature. Finally, a relatively narrow and intense line is restored, whose location is largely displaced with respect to the initial location, corresponding to $\delta = 0.08$ [$\vec{k} = (0.270, 0.270, 0.5)$].

Such a behavior can be understood if one assumes that a discontinuous transition takes place at T_{II}. The above observations would then denote the progression of the upper phase with $\delta \simeq 0.08$, while the lower one with $\delta \simeq 0.025$ regresses. The intermediate curves in Fig. 5 would be produced by the coexistence of the two types of satellites which are

not resolved since their interval is only slightly larger than the instrumental width.

With regard to the insufficient q resolution of the experiment and the possibility of a temperature gradient in the sample, we cannot exclude the occurrence of a continuous, though necessarily steep, variation of δ near T_{II}. However, the discontinuous process seems more likely, since a differential thermal analysis (DTA) measurement in the same sample reveals a latent heat peak at T_{II} of approximately 0.02 cal/g. As shown by Figs. 3–5, the transition at T_{II} also provokes a variation of the width and intensity of the satellites.

Phase I, which is stable above T_{II}, is mainly characterized by a strong temperature dependence of δ (Fig. 2). Its value increases linearly from 0.080 up to 0.125 at $\simeq$290 °C [$\vec{k}$=(0.281,0.281, 0.5)]. It then remains constant.

It was pointed out previously[21] that the upper limit of stability of the incommensurate phase cannot be located accurately from the sole consideration of the vanishing of the satellite's intensity. As illustrated by Fig. 4, the intensity plot has a tail and goes to zero asymptotically. This blurring, which also prevents a safe assignment of the thermodynamic order of the transition, is due to the fact that in the transition region, the elastic scattering is superimposed with quasielastic diffuse scattering produced by the fluctuations of the order parameter, and whose intensity peaks at T_I.

We have nevertheless been able to locate T_I in the neutron data by combining the following converging observations.

(i) A steep increase of the q width of the scanned peak is observed above 288 °C, while below this temperature the width is almost constant. Such a behavior is consistent with the decrease of the correlation length above the transition.

(ii) Both plots of δ (Fig. 2) and the satellite's intensity (Fig. 4) show that a thermal hysteresis between the heating and cooling measurements starts at 288±5 °C. On the other hand, the variations of the optical birefringence measured in the same sample (Fig. 6) indicate that this hysteresis, with the same qualitative shape, starts at the vanishing point of the birefringence, i.e., at the transition temperature between the tetragonal and orthorhombic phases which coincides with T_I.

(iii) If we extrapolate in the plot of the satellite's intensity the rectilinear portion recorded between 260 °C and 280 °C we obtain a temperature of vanishing at 290±4 °C.

We can therefore assign to T_I the value 288

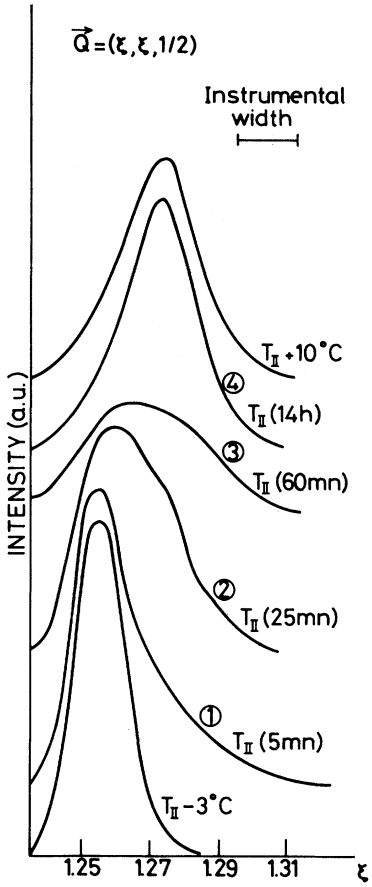

FIG. 5. Evolution with time of the q-spectrum of the

$$\left[1+\frac{1+\delta}{4}\quad 1+\frac{1+\delta}{4}\quad \frac{3}{2}\right]$$

satellite along the modulation direction after setting temperature at $T_{II}\simeq$250 °C.

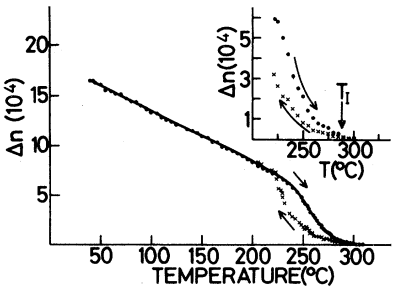

FIG. 6. Temperature dependence of the birefringence Δn in the (001) plane on heating and on cooling. The insert specifies the variations and the form of the thermal hysteresis near T_I. On heating no discontinuity is observed at T_{II}.

± 2 °C. As shown by Fig. 2, this temperature is the borderline between the range where δ is constant ($T > T_I$) and the range where δ varies linearly ($T_{II} < T < T_I$).

Thus, except possibly for a few degrees Centigrade below T_I, δ varies in the whole range of stability of phase I. This behavior contrasts with that of many incommensurate substances for which the region of constancy of δ occupies a large fraction of the incommensurate phase below T_I. However, variations similar to the present variations have been observed previously, for instance, in K_2ZnCl_4.[22]

The order of the T_I transition cannot be safely asserted on the basis of the neutron data, though the behavior near T_I suggests that it is second order or weak first order. This order can more accurately be determined from other physical measurements. In this respect, the vanishing of the birefringence appears perfectly continuous. On this basis the transition can be assigned as second order. Consistently no thermal effect could be detected at T_I in a DTA heating run.

As already pointed out in Ref. 12, the occurrence of a large thermal hysteresis appears contradictory with a second-order or even a weak first-order transition. This contradiction will be discussed in the next section. The hysteresis consists of a major qualitative difference between the heating and cooling runs. Up to 50 °C additional cooling is needed to reach the same value of a quantity as in the heating run. In addition, no counterpart of T_{II} was observed in the cooling run, the properties all apparently varying in a continuous way. This hysteresis, which affects the satellite's position and intensity, had also been noted previously as a permanent feature of BSN, which is observed in the measurement of any physical property (shear strain, birefringence, elastic constants), and in any sample. The lower temperature at which the heating and cooling runs merge again lies in the range (100–200 °C), and seems to depend on the speeds of the heating and cooling runs.

The static results deduced from the neutron scans are in good qualitative agreement with those obtained in the x-ray study.[12] Quantitatively, the neutron data have supplied more accurate values of the variations of δ. In particular, the RT value of this parameter was at the limit of accuracy of the x-ray experiment. On the other hand, the linear variation of δ between T_{II} and T_I did not appear clearly in the previous data.

The most important difference concerns the location of the T_I and T_{II} temperatures. These were found, respectively, at 305 °C and 275 °C in the x-ray measurements. The shift of T_I is not unexpected since the x-ray sample had a composition closer to the stoichiometric one. The downward shift recorded here for a barium-rich sample is in agreement with the composition phase diagram previously known for the tetragonal-orthorhombic transition on the basis of Raman and birefringence measurements.[10,19] The present neutron data suggest that besides shifting T_I, the deviation from stoichiometry has the effect of widening the range of stability of phase I from 30 °C to 38 °C.

The x-ray experiment had disclosed weak reflections at room temperature nearby the expected location of second-order satellites. This location is

$$\left[h \pm \frac{1+\delta}{2} \quad h \pm \frac{1+\delta}{2} \quad l\right].$$

Thus, one should find pairs of satellites placed symmetrically on either side of $(h+\frac{1}{2}\ h+\frac{1}{2}\ l)$ positions and separated by 2δ in the [110] direction. However, these two reflections are second satellites of different main reflections, and they are likely to possess different intensities. Besides, they will only be distant enough from each other to be resolved above T_{II}.

Systematic neutron scans in the vicinity of $(h+\frac{1}{2}\ h+\frac{1}{2}\ l)$ positions have led to the observation of a few weak reflections ($\sim 1\%$ of strong first satellites at RT centered on the former position with no apparent structure at RT. The most intense ones were found near (2.5 2.5 0) and (3.5 3.5 1). Their width was significantly larger at RT than the instrumental resolution, in contrast to the width of first satellites. Quantitatively, this width was consistent with the presence of two satellites separated by 2δ (Fig. 7).

On heating, their intensity decreased sharply (approximately as the third power of first satellites). In phase I, where the larger value of δ would have allowed their doubtless identification, no intensity could be detected at the corresponding positions.

B. Dynamical behavior

The presence of diffuse scattering in the transition region has been found both in the elastic neutron spectra and in the x-ray photographs. It shows that precursor effects of the T_I transition exist in BSN. To probe their possible dynamical

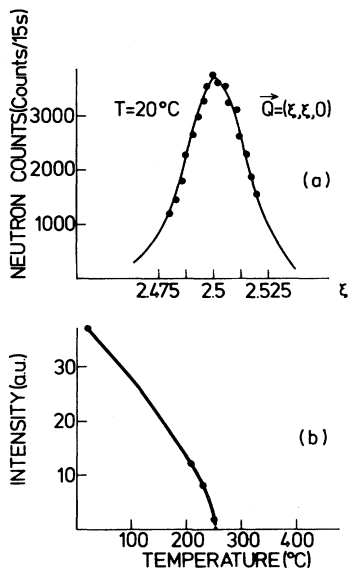

FIG. 7. (a) Profile of the elastic scattering scanned along [110] showing peak centered at $(h+\frac{1}{2},h+\frac{1}{2},0)$ which could correspond to a second-order satellite. (b) Temperature dependence of the intensity of the cor responding reflection.

nature, the behavior of the low-lying excitations has been examined by performing inelastic neutron scans near the vector

$$\left(4-\frac{1+\delta}{4},4-\frac{1+\delta}{4},\frac{1}{2}\right),$$

which corresponds to one of the strongest satellites observed in the $(1\bar{1}0)$ scattering plane. Measurements in this plane were also performed at several vectors on the line joining $(3.5\,3.5\,\frac{1}{2})$ (A point) and $(4\,4\,\frac{1}{2})$ (Z point) in order to determine the dispersion curve of the excitations in the direction of the modulation. On the other hand, inelastic scans were achieved near (0 5.5 2.5) in the most intense of the accessible diffused scattering rods revealed by the x-ray photographs at mid-distance between two satellites (Fig. 1). These rods lie approximately along the $[1\bar{1}0]$ direction. They are significantly curved, and their curvature depends on temperature. Consequently it was not possible to find a scattering plane containing the rod, and the inelastic scans were only probed at one point of the rod, away from the satellites.

Let us first examine the results at the critical wave vector $\vec{k}_c$. This vector corresponds, above T_I, to the maximum of the scattered intensity obtained in the q-scans along the [110] direction. Its location was found to be temperature independent at $\vec{k}_c = (3.72\,3.72, 0.5)$. Below T_I, $\vec{k}_c$ corresponds to the temperature-dependent position of the satellite reflection. Figure 8 shows the energy scans between 220 °C and 660 °C, while Fig. 9 reproduces the scans obtained slightly above T_I.

For $T > T_I$, the plots reveal the presence of a soft-phonon mode as well as that of a central component with a critical behavior. Thus at the highest temperature reached (660 °C) the energy scans display peaks at $|\Delta E| \approx 0.75$ THz and at $\Delta E \approx 0$. The width of the first one (~ 0.5 THz) is much larger than the instrumental resolution. This peak can be assigned to a damped phonon with low frequency. The central component is narrow and its width appears to be determined by the instrumental resolution.

As the temperature is lowered the phonon peak is shifted towards lower energies. Below 400 °C no relative maximum can be resolved for it, and its

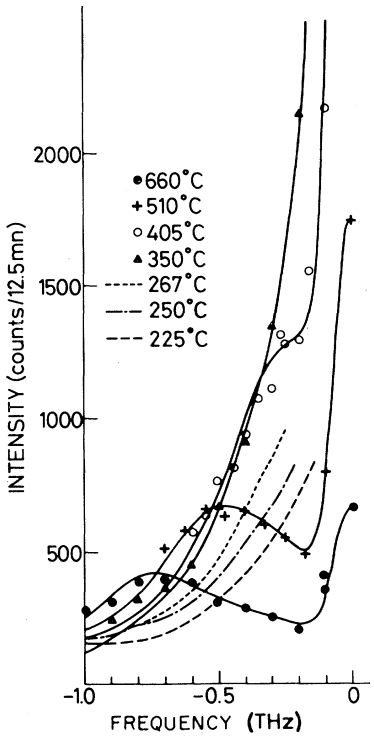

FIG. 8. Energy scans at the critical wave vector $\vec{k}_c$ (see text) showing the occurrence of a soft-phonon mode and of a central peak above T_I. The solid curves are a fit of the experimental points using Eq. (4) and a Gaussian central peak. Interrupted lines outline the evolution below T_I.

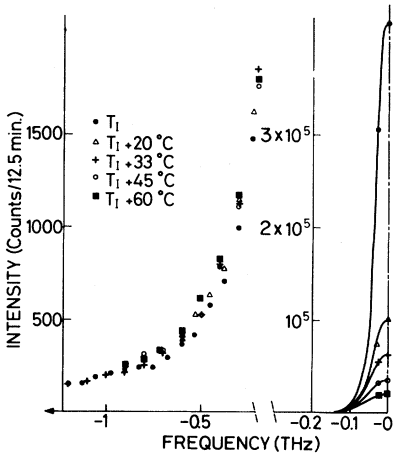

FIG. 9. Energy scans at $\vec{k}_c=(3.72,3.72,0.5)$ showing the temperature independence of the phonon side band ($\Delta E>0.2$ THz) between T_I and ~ 350 °C, while the central peak diverges steeply in the same temperature range.

contribution to the energy scans takes the form of a broad tail characteristic of an overdamped phonon. This overdamping persists below T_I, and the only variations recorded in the lower phases are a decrease of the intensity of the side bands on cooling away from T_I.

On the other hand, the main feature of the central component is a steep increase of intensity on approaching T_I from above. At the onset of the incommensurate phases this quasielastic scattering can no longer be studied at $\vec{k}_c$ due to the presence of the Bragg reflection.

Thus, the dynamical behavior of BSN appears qualitatively similar to the one observed at a number of structural transitions with a dynamical response constituted by a soft mode and a critically diverging central peak. It is worth noting that no anomaly of behavior has been observed at $\simeq 580$ °C, i.e., at the ferroelectric transition, whose mechanism does not seem to interact with that of the considered transition.

Above 400 °C the phonon peak is resolved, and the respective contributions of the two former features can be separated through a fit of the energy scans. As the central component has the instrumental width, we have assumed that it has a Gaussian shape.[23] On the other hand, the soft-mode response has been fitted to that of a damped harmonic oscillator[24]:

$$I(\omega,T)=\frac{A\gamma_0 T}{(\omega^2-\omega_\infty^2)^2+\gamma_0^2\omega^2} . \tag{4}$$

The fit shows that for energy transfers greater than 0.2 THz the central peak has a negligible contribution, and that the scans are entirely determined by the soft phonon (once the incoherent scattering is substracted). Examination of the scans between T_I and 350 °C suggests that this result actually holds in the whole range of temperatures above T_I, as illustrated by Fig. 9. In this plot the central component's intensity varies by a factor of 20 while the broad tail beyond 0.2 THz is almost unaffected. Accordingly, we have used Eq. (4) to fit the inelastic scans between T_I and 660 °C, not only in the temperature range where the phonon peak can be resolved. Considering the width of the phonon peak (over 0.5 THz) the scans were not corrected for the instrumental width. Below T_I, the experimental data are less precise. Moreover, the dynamical response is expected to consist of several excitations. Therefore no fit of the broad side-band has been attempted in this range of temperature.

The results of the fit of the phonon behavior show that the damping factor γ_0 in Eq. (4) is almost constant in the whole range of temperatures explored. We have

$$\frac{\gamma_0}{2\pi}=0.65\pm 0.05 \tag{5}$$

expressed in THz. In contrast, the frequency $\omega_\infty/2\pi$ decreases markedly from 0.85 THz (28 cm^{-1}) at 660 °C down to 0.39 THz (13 cm^{-1}) at 350 °C. As already mentioned (Fig. 9), below this temperature the phonon contribution seems to remain constant, thus suggesting that ω_∞ approaches a value close to that determined at 350 °C.

The changing of regime from an underdamped oscillator to an overdamped one occurs at 385 ± 15 °C. It appears essentially due to the softening of ω_∞, while the intrinsic damping remains constant.

The saturation of the temperature dependence of ω_∞ on approaching T_I agrees with the observations in other transitions in which the soft phonon interacts with a relaxing degree of freedom giving rise to a central peak. In this case one expects on the basis of a phenomenological model[24] that the inverse static susceptibility $\chi\sim 1/\omega_0^2$ will vanish at T_I. As stressed by various authors[25] the temperature dependence of ω_0 can be reached through measurement of the total intensity I scattered in both the central peak and the soft mode peak. We have

$$\omega_0^2 \sim \frac{T}{I} . \tag{6}$$

The experimental values of ω_0^2 are plotted in Fig. 10 as well as those of ω_∞^2. We have scaled the variations to each other at 660 °C by using the relation[24]

$$\omega_\infty^2 = \omega_0^2 \left[1 + \frac{I(\text{central peak})}{2I(\text{phonon})} \right] , \tag{7}$$

which provides a difference of 3% between the two frequencies at this temperature. Between T_I and 350 °C, in the region where the phonon contribution to the total intensity is small, the variations of ω_0^2 were deduced from measurements of the integrated intensities at two distinct locations in reciprocal space, near (3.72 3.72 0.5) and (1.28 1.28 1.5). In this region, Fig. 10 shows that the variations of ω_0^2 are in good agreement with a linear law:

$$\left(\frac{\omega_0}{2\pi} \right)^2 = (0.0136 \pm 0.001)(T - T_I) \tag{8}$$

expressed in THz^2. Above 350 °C the linear law is no longer satisfactorily obeyed, with ω_0^2 increasing more steeply on heating. This behavior is surprising, as one would rather expect a decreasing slope due to the interaction of the soft mode with excitations lying at higher energies. The variations of ω_∞^2 are parallel to those of ω_0^2 down to 350–400 °C below which the mentioned leveling takes place.

The fitting of the phonon behavior used for the critical wave vector has been extended to the energy scans at $\vec{k} \neq \vec{k}_c$. These scans are reproduced in Fig. 11 for some selected points neighboring $\vec{k}_c$. They also involve a phonon peak and a central peak. However, the softening of the phonon and the intensity divergence of the central peak are less pronounced as one gets farther from $\vec{k}_c$. Thus at the Z point $(44\frac{1}{2})$ the maximum of the phonon peak is almost temperature independent.

The set of fitted ω_∞ frequencies obtained for various $\vec{k}$ vectors along the [110] direction or in the diffused scattering rod determine the shape of the dispersion surface of the phonon branch in the $(\eta\xi\frac{1}{2})$ plane. The section of this surface by the $(1\bar{1}0)$ plane, containing $\vec{k}_c$, is reproduced in Fig. 12. At 660 °C, the curve is already significantly hollowed near $\vec{k}_c$, and it deepens as T_I is approached. The extension of the softening along the direction of the modulation appears more restricted to the vicinity of $\vec{k}_c$ than in the cases of other incommensurate substances such as K_2SeO_4 or $BaMnF_4$. We have not attempted to construct the dispersion curve relative to the uncoupled mode ω_0

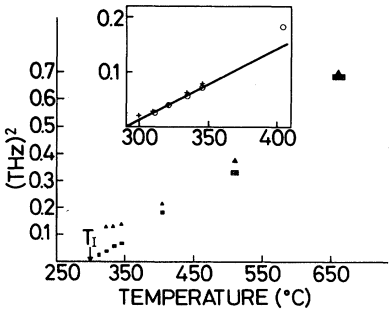

FIG. 10. Variations of the squared frequencies of the undamped renormalized soft mode, ω_∞^2 (filled triangles) and ω_0^2 (squares) proportional to the inverse static susceptibility of the system (Ref. 24). The inset shows the experimental points for ω_0^2 deduced from measurements in two different Brillouin zones (crosses and circles) in a range of 60 °C above T_I.

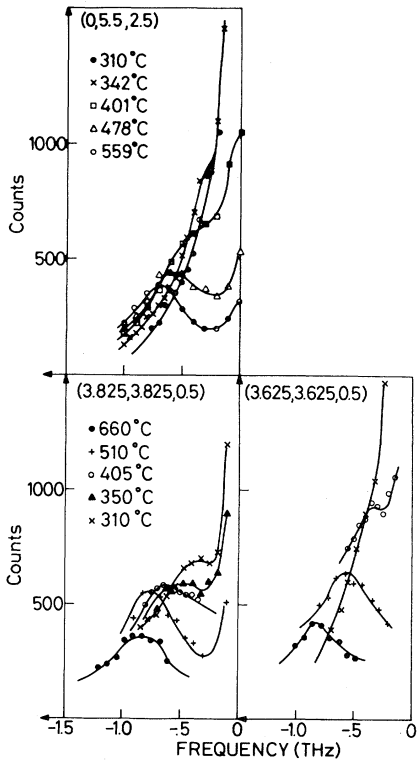

FIG. 11. Energy scans at points neighboring $\vec{k}_c$ along the modulation vector and in the diffused scattering at mid-distance between two satellites.

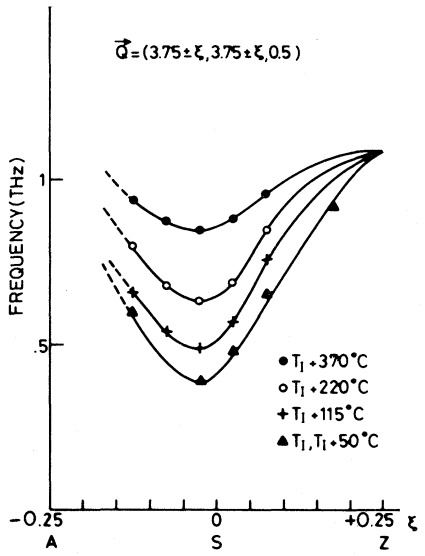

FIG. 12. Dispersion curve of the soft-phonon branch along the [110] direction.

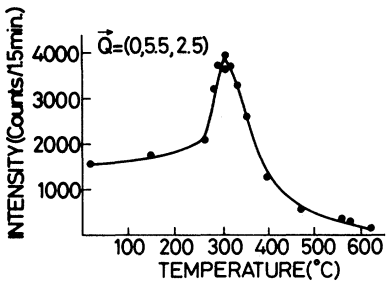

FIG. 13. Temperature dependence of the central peak intensity in the diffused scattering near the R point of the Brillouin zone.

for lack of sufficient data on the central peak at $\vec{k} \neq \vec{k}_c$.

In the $[1\bar{1}0]$ direction of the diffused rods, the behavior is different. A strong temperature dependence of the soft mode is observed (Fig. 11) at mid-distance between satellites (near the R point of the Brillouin zone) and therefore exists in the whole rod. This section of the dispersion surface perpendicular to $\vec{k}_c$ is very flat. Thus, at $\sim 350\,^{\circ}\mathrm{C}$ the frequencies at $\vec{k}_c$ and near the R point are, respectively, 0.4 and 0.55 THz. However, the temperature interval in which the soft mode is overdamped is narrower. This regime starts below $\sim 360\,^{\circ}\mathrm{C}$ and stops at $\sim 200\,^{\circ}\mathrm{C}$. Below the latter temperature the soft mode can be resolved again, and it hardens up to $\simeq 1$ THz at room temperature.[11] The central peak contribution is less important than that at $\vec{k}_c$. It can be followed below T_I and it is observed to decrease by a factor of 3 and then to remain almost constant down to room temperature (Fig. 13).

On the basis of these results, the nature of the diffused scattering observed in the x-ray experiment is clarified. Close to the critical wave vector $\vec{k}_c$ and near T_I it is essentially due to the quasi-elastic scattering (central peak) distinct from the overdamped phonon contribution. On going away from $\vec{k}_c$ in the $[1\bar{1}0]$ direction the contribution of the soft phonon increases and becomes an important fraction of the scattering. Over 100 °C above T_I, the diffused rods essentially reflect the valley-shaped dispersion surface of the soft-phonon branch.

IV. DISCUSSION

The dynamical measurements have shown that the loss of stability of the high-temperature phase involves a soft lattice mode that is underdamped $\sim 100\,^{\circ}\mathrm{C}$ above T_I. Its occurrence suggests that the incommensurability in BSN is, at least partly, a displacive one. Let us specify the microscopic nature of the incommensurate displacements and relate, on a phenomenological basis, the neutron scattering results to the macroscopic properties already studied in BSN.

A. Microscopic nature of the incommensurability

As mentioned above, structural data on BSN are only available at room temperature.[16] Furthermore, the structure has been worked out without taking into account the satellite reflections. It is nevertheless expected to contain informations on the modulation: De Wolff has pointed out[26] that the main reflections provide the "average" structure of the incommensurate phase which is distinct from the basic structure of the high-temperature phase. In the average structure the modulated displacement of an atom will appear as a blurred cloud of electronic density extending to the whole set of positions occupied by the atom in the incommensurate structure. For instance, an analysis of the main reflections of Na_2CO_3 has provided[27] a structure in which certain atoms are split between

two positions. Such a situation will also be encountered for a commensurate superstructure if the superlattice reflections are neglected. Actually, this type of splitting has been observed in BSN. The RT structure determined by Jamieson *et al.*[16] shows that all the oxygen atoms situated in the $z=\frac{1}{2}$ plane are split between two positions whose separation range from 0.283 to 0.556 Å. In a minor way this splitting affects part of the barium atoms. We can therefore assume that the incommensurate or nearly commensurate modulations, respectively, detected in phases I and II are due to the displacements of the preceding oxygen and barium atoms at microscopic level. Such an assumption is consistent with the remark of Jamieson *et al.*[16] that the orthorhombic distortion of the lattice, which takes place at T_I, is primarily related to the occurrence of the atom splittings. The amplitudes of the modulated displacements can be taken equal to half the distance between split atoms. Figure 14 provides a schematic description of the displacements in the tetragonal unit cell. It appears that the modulation consists mainly in a collective shearing of the oxygen octahedra, in which the basis of each octahedron in the *ab* plane is fixed while the oxygen at the upper and lower vertices move parallel to this plane in opposite directions. This alternation along the *z* axis corresponds to the doubling of periodicity along this direction. The displacements have a predominant component along the *a* orthorhombic axis, which is also parallel to the direction of the modulation. The overall amplitude in Å of the modulation at RT is

$$\left[\sum x_i^2\right]^{1/2} \simeq 0.8 \ , \tag{9}$$

where the x_i are the displacements of the oxygen atoms in the tetragonal unit cell.

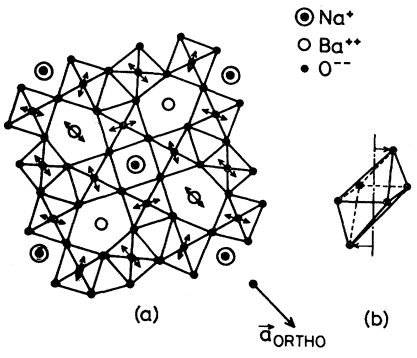

FIG. 14. Schematic representations of the distortions occurring in the tetragonal unit cell (a) and of the shearing of an oxygen octahedron in the structure (b). The moving atoms are all in the $z=\frac{1}{2}$ plane, while the fixed oxygen atoms lie in the $z=0$ plane (after Ref. 16). (a) represents a projection of the RT structure on the *ab* plane, while (b) has the *c* axis vertical.

In the first approximation, we can expect that the soft mode detected above T_I consists of the same collective shearing of the oxygen octahedra. As noted by Dorner *et al.*[25] a slight difference can, however, exist between the static displacements below a transition and the instantaneous displacements of the driving phonon mode due to the onset below T_I of secondary degrees of freedom coupled to the main one.

The valley-shaped dispersion surface of the soft phonons which gives rise to the diffused scattering rods reveals the occurrence of strong correlations in the *ac* orthorhombic plane. This plane contains the modulation vector and the polar *c* axis. The possible structural basis for a correlation along the *c* direction could be the fact that in an oxygen octahedron the motions of the upper and lower vertices in the same direction or in opposite ones are not equivalent, the latter motion being energetically favored. This feature will establish strong correlations in the chains of oxygen octahedra parallel to $\vec{c}$ through the corner sharing of the consecutive octahedra. In contrast, no obvious microscopic mechanism accounts for the correlation along the [110] direction. However, it is likely that this correlation is due to the same interactions which provoke the onset of the long-range incommensurate order in this direction and which are not perceived clearly at present.

B. Order parameter associated with the modulation

The collective shearing of atoms constituting the modulated displacement coincides with the frozen-in components of the order parameter below T_I. The complete characteristics of this quantity can be worked out on the basis of symmetry considerations.

For a given modulation vector $\vec{k}$, the symmetry properties of the order parameter are described by an irreducible representation $\Gamma_m(k^*)$ of the high-symmetry space group G_0. k^* is a star of vectors of the first Brillouin zone containing the modulation vector $\vec{k}$. The index m specifies a small representation of the little group $G_{\vec{k}}$ associated with $\vec{k}$.

As the modulation vector is temperature dependent below T_I, one has to deal with a whole set of order parameters differing by their star but having in common the same type of small representation.

The high-symmetry phase of BSN, stable above T_I, has the $4mm$ point symmetry.[1] Its space group G_0 has not yet been investigated in details. However, on the basis of the available data, there is little doubt that this group is $P4bm$ with parameters $a_t \simeq 12.4$ Å, $c_t \simeq 4$ Å. Three types of data support this assignment. In the first place, $P4bm$ is the space group which describes the symmetry of the tetragonal polar phase for all the members of the tungsten-bronze family in which this symmetry appears reliably determined, such as, for instance, potassium lithium niobate.[28] On the other hand, $P4bm$ constitutes a pseudosymmetry of the RT average structure of BSN.[14] Finally, the systematic extinctions expected for this group, i.e., $(2h+1\ 0\ l)$ and $(0\ 2h+1\ l)$ are consistent with the partial x-ray[12] measurements and the present neutron scattering measurements performed above 300 °C. In these measurements only a very weak intensity can be detected for the forbidden reflections, which is systematically 1—3 orders of magnitude smaller than the intensity of permitted reflections. Taking these reflections into account would lead to the $P4mm$ space group, which is clearly incompatible with the RT structure. It is thus likely that the slight departure from a complete extinction is due to the nonstoichiometry of the samples, which perturbs the selection rules and that the relevant space group G_0 is indeed $P4bm$.

The star $\{k^*\}$ containing the modulation vector $\vec{k}=\vec{k}_+$ is composed of four arms

$$\{k^*\}=\pm\left[\frac{\vec{a}_t^*\pm\vec{b}_t^*}{4}(1+\delta)+\frac{\vec{c}_t^*}{2}\right]=\pm\vec{k}_\pm\ . \tag{10}$$

Their extremities are located on the Brillouin-zone boundary. The small group $G_{\vec{k}}$, whose point group is $m_{\bar{x}y}$, has two small-representations τ_1 and τ_2 both one dimensional. Their characters for the element

$$\left[m_{\bar{x}y}\left|\frac{\vec{a}+\vec{b}}{2}\right.\right]$$

are, respectively

$$\exp\left[\frac{i\pi(1+\delta)}{2}\right]\quad\text{and}\quad\exp\left[\frac{-i\pi(1+\delta)}{2}\right].$$

Thus, the order parameters corresponding to the incommensurate phase of BSN are four dimensional and have one of two possible symmetries, $\Gamma_1(k^*)$ or $\Gamma_2(k^*)$. A further specification of this symmetry is actually possible on the basis of the available crystallographic data.

At RT, the modulation is very close to a commensurate one ($\delta\approx 0$) corresponding to a fourfold multiplication of the unit cell. Accordingly, we can examine the experimental data in the approximation that they describe a superlattice structure. For the considered fourfold-cell expansion, each of the Γ_i representations determines two possible orthorhombic space groups indicated in Table I. Careful reexamination of RT precession x-ray photographs[12] performed on single domain plates of BSN (Ref. 29) shows that the observed systematic extinctions match only one of these groups, labeled $Bbm2$, which thus constitutes the approximate space group of the RT structure (including the satellite reflections). This group also appears consistent with the atomic configuration of Jamieson's RT structure,[16] while two of the other possible groups in Table I, such as $Bmm2$, would require certain oxygen atoms with $z=\frac{1}{2}$ to have no split positions. The preceding identification allows one to assert that the order parameter of BSN has $\Gamma_1(k^*)$ symmetry.

Few nonmagnetic transitions, other than BSN, possess a four-component order parameter. In particular, the incommensurate phases in insulators were generally described, with the exception of $BaMnF_4$, by two-component order parameters. Let us examine the specific consequences of this order parameter symmetry by working out its associated free-energy.

C. Free-energy density and ferroelastic behavior in BSN

Standard methods[30] determine the following form for the homogeneous order-parameter expansion truncated to the fourth-degree terms:

$$\begin{aligned} f_1=&\frac{\alpha}{2}(\rho_1^2+\rho_2^2)+\frac{\beta_1}{4}(\rho_1^4+\rho_2^4)\\ &+\frac{\beta_2}{4}\Delta(\delta)[\rho_1^4\cos(4\phi_1)+\rho_2^4\cos(4\phi_2)]\\ &+\frac{\beta_3}{2}\rho_1^2\rho_2^2\ , \end{aligned} \tag{11}$$

where ρ_1,ϕ_1 and ρ_2,ϕ_2 are the respective modulus

TABLE I. Possible commensurate low-symmetry phases induced by the representations Γ_1 and Γ_2 corresponding to the star of $\vec{k}$ vector $\pm k_{\pm}$. Only one of the possible equivalent orientations (domain) of each phase is indicated. The multiplication of the primitive unit cell is indicated in the last column while the preceding column shows the standard crystallographic multiple cell. In BSN the low symmetry phase agrees with the prediction for Γ_1.

Order-parameter components				Sponteneous strain	Space groups induced by		Multiple unit cell	Primitive cell expansion
ρ_1	ϕ_1	ρ_2	ϕ_2	e_1-e_2	Γ_1	Γ_2		
ρ	0	0	0	yes	*Bbm*2	*Bba*2	$2(\vec{a}+\vec{b})$ $(\vec{b}-\vec{a})$	4
ρ	$\frac{\pi}{4}$	0	0	yes	*Bmm*2	*Bma*2	$2\vec{c}$	
ρ	0	ρ	0	no	*I*4	*I*4	$2(\vec{a}-\vec{b})$ $2(\vec{a}+\vec{b})$	8
ρ	$\frac{\pi}{4}$	ρ	$\frac{\pi}{4}$	yes	*Imm*2	*Iba*2	$2\vec{c}$	

and phase of the components of the order parameter spanning $\pm\vec{k}_+$ and $\pm\vec{k}_-$. The modulated nature of ρ_i and ϕ_i derives from the fact that their translational symmetry is described by an "incommensurate star" $\pm\vec{k}_{\pm}$. The coefficient $\Delta(\delta)=0$ for all values of the modulation vector $-1<\delta<1$ except for the "commensurate" vector $\delta=0$. The corresponding term is the only one in f_1, which displays an anisotropy with respect to the phases ϕ_i. In the framework of existing phenomenological theories this is the "lock-in" term whose presence favors the stabilization of a commensurate phase with a superlattice periodicity. On the basis of the fourth degree expansion, $\vec{k}_0=(\frac{1}{4},\frac{1}{4},\frac{1}{2})$ is the only possible lock-in vector. In the neighborhood of the initial value of the modulation ($\delta\simeq 0.125$) other positions of lock-in, such as $(\frac{1}{3},\frac{1}{3},\frac{1}{2})$ appear less likely since they would be stabilized by terms of degrees higher than 4.

The order-parameter expansion (11) is identical to that considered by Mukamel *et al.*[31] for the phase transitions of DyC_2 and NbO_2. These authors have shown, in the framework of the renormalization-group method, that it is associated with a stable fixed point. It is therefore compatible with the occurrence of a continuous transition, in agreement with our experimental assignment of the T_I transition. Such a situation is exceptional since the transitions possessing an order parameter with more than three components are generally conjectured[31] to be driven to first order by the fluctuations. This is the case, in particular, for $BaMnF_4$.[32] The theoretical exponents $\beta\approx 0.39$ and $\gamma\approx 1.39$ which are expected to govern the critical behavior of BSN have been worked out by Mukamel.[31] Their comparison with the experimental data seems premature. In the first place, our data are insufficiently accurate in the vicinity of T_I. The satellite's intensity, controlled by the exponent 2β, is strongly perturbed by the diffused scattering. Also, the indirect determination of ω_0^2 through integration of the diffused scattering does not warrant a sufficient precision very close to T_I. On the other hand, we note that the anisotropic shape of the fluctuations, disclosed by the scattering rods, is identical to that observed in NbO_2. For this material it was pointed out by Pynn *et al.*[33] that due to this anisotropy, the critical behavior could correspond to ($n=2$, $d=2$) rather than the former ($n=4$, $d=3$). The fact that ω_0^2 follows a linear law between $T_I+10\,^\circ C$ and $T_I+60\,^\circ C$ fits neither of these theoretical situations. In this range of temperatures, it is likely that the critical behavior is strongly influenced by the presence of defects, related to the nonstoichiometry of the samples, and whose important role in the static behavior of BSN is discussed in the following paragraph.

Below T_I, the free-energy (11) has two possible sets of minima for any value of δ. One corresponds to $\rho_1=\rho_2\neq 0$ and is realized for $\beta_1>|\beta_3|$. It involves the onset of spontaneous values for components of the order parameter relative to the four arms of $\{k^*\}$, i.e., of modulations with equal amplitudes along both the a and b directions. The other is $\rho_1\neq 0$, $\rho_2=0$ (alternately $\rho_2\neq 0$, $\rho_1=0$), stable for $\beta_3>\beta_1>0$, and corresponds to a single modulation either along $\vec{a}$ or along $\vec{b}$. For $\delta=0$, these modulations become superstructures with,

respectively, eightfold and fourfold unit-cell expansions. The presence of the phase-dependent term lifts the phase degeneracy and gives rise, for each of the preceding states, to two unequivalent states, with $\cos 4\phi_i = \pm 1$ (Table I).

BSN has a single modulation and therefore corresponds to $\rho_i \neq 0$, $\rho_j = 0$. The frozen-in structural displacements described in Sec. IV A are associated to a single direction in the space spanned by the two first components of the order parameter. This direction is undetermined in the modulated phase. For $\delta = 0$, it settles along one of the axes $[\phi_i = 0, \text{mod}(\pi/2)]$ in this space. The exchange of $\rho_1 \neq 0$ and $\rho_2 \neq 0$ corresponds to the switching from one ferroelastic domain to the other, the two domains having mutually perpendicular directions of modulation.

The main macroscopic anomalies accompanying the onset of the incommensurate phase are the occurrence of the ferroelastic spontaneous shear and a softening of the elastic constants along C_{11} and C_{22}.[13,15] Their mechanism relies on the coupling of the strain components to the order parameter. The contribution of these components to the free-energy is

$$f_2 = \frac{C_{11}}{2}(e_1^2+e_2^2) + C_{12}e_1e_2 + C_{13}(e_1+e_2)e_3 + \frac{C_{33}}{2}e_3^2 + [\mu_1(e_1+e_2)+\mu_3 e_3](\rho_1^2+\rho_2^2) + \nu(e_1-e_2)(\rho_1^2-\rho_2^2) , \quad (12)$$

where the tensorial quantities refer to the orthorhombic axes. We have omitted the dielectric polarization component P_c along $\vec{c}$, which is coupled in the same way as e_3. This omission is legitimate provided that elastic constants in (12) are considered as renormalized by the strong piezoelectric coupling which exists in BSN.

The striking characteristics of Eq. (12) is that the coupling of the strain to the order parameter does not depend on ϕ_i. For $\rho_i \neq 0$, $\rho_j = 0$, the macroscopic symmetry will be broken through the onset of $e_1 - e_2 \sim \rho_i^2$, and an orthorhombic symmetry will be established both in the incommensurate case ($\delta \neq 0$) and in the commensurate case ($\delta = 0$). No change of macroscopic symmetry is expected from the locking-in of the modulation at a commensurate value. This situation contrasts with the cases of most incommensurate phases studied up to now for which the average point symmetry of the incommensurate phase was identical to that of the high-temperature phase and different from that of the commensurate one. This peculiarity of BSN relies partly on the unusual number of components of the order parameter. Thus for the common two-component case, the modulus ρ^2 is totally symmetric, and the symmetry-breaking macroscopic components are necessarily coupled to a phase-dependent term whose space average is zero in the incommensurate phase.

In the framework of Landau theory,[14] Eq. (12) determines a temperature dependence of the shear strain, identical to that of ρ^2. This dependence should therefore be the same as that of the integrated intensity of the satellite reflections. The measurements of $e_1 - e_2$, which have been obtained by a γ-ray diffractometric technique,[34] agree qualitatively (Fig. 4) with this prediction.

Equation (12) also shows that, if the modulation affects exclusively the phases ϕ_i, the macroscopic behavior of BSN will be identical to that of an improper ferroelastic. Accordingly the results previously worked out for BSN,[14] on the assumption that the transition at T_I was an improper ferroelastic transition between crystalline phases will hold without modification. The role played in the former theory by the two homogeneous components of a two-dimensional order parameter is taken here by the two homogeneous moduli ρ_1 and ρ_2 associated with a four-dimensional order parameter. This theory was able to account qualitatively for the macroscopic behavior of BSN, and, in particular for the anomalous increase, on heating towards T_I, of the difference $C_{22} - C_{11}$ between elastic constants.

D. Incommensurate behavior in BSN

The experimental observations relative to the static properties have shown that the behavior of BSN complies partly with the standard pattern which is expected for incommensurate structures.[35] Thus BSN undergoes a sequence of two transitions. The one at T_I is continuous and relates the high-symmetry phase with the incommensurate phase labeled I. The other one at T_{II} is discontinuous and associated with an abrupt jump of the modulation wavelength. In phase II the modulation vector approaches the "commensurate vector" $\vec{k}_0 = (\frac{1}{4}, \frac{1}{4}, \frac{1}{2})$. On the other hand, two striking nonstandard features have been found: an incompleteness of the locking in below T_{II} with the persistence of an almost temperature-independent incommensurability, and a large difference between

the heating and cooling data. This difference starts at the continuous transition T_I, and includes a smeared behavior of all the quantities in the cooling process. Let us first consider the standard aspects of the incommensurate phase in BSN.

These aspects are usually accounted for by a phenomenological model based on an extension of the Landau theory for the considered transitions. This model has mainly been studied for transitions having an order parameter of smaller dimension. Let us examine along the same lines the characteristics of the four-component expansion (11). In this equation, the coefficients are functions of δ. To avoid the manipulation of a $\vec{k}$-dependent free-energy, we can, following a method used by Levanyuk *et al.*,[36] refer the order parameter to the special $\vec{k}_0$ vector associated to $\delta=0$, and consider that the ρ_i and ϕ_i are functions of the spatial coordinates. Additional terms f_3 must then be added to the free-energy density, containing the spatial derivatives of the order-parameter components. Consistent with experimental observations, symmetry considerations show that the z coordinates can be ignored: No bilinear product of the order parameter and of its first derivative with respect to z can contribute to f_3.[36] Referring the x and y coordinates to the orthorhombic axes and limiting f_3 to quadratic terms in the order parameter components, we obtain

$$f_3=\lambda\left[\rho_1^2\frac{\partial\phi_1}{\partial x}+\rho_2^2\frac{\partial\phi_2}{\partial y}\right]+\kappa_1\left[\rho_1^2\left[\frac{\partial\phi_1}{\partial x}\right]^2+\left[\frac{\partial\rho_1}{\partial x}\right]^2+\rho_2^2\left[\frac{\partial\phi_2}{\partial y}\right]^2+\left[\frac{\partial\rho_2}{\partial y}\right]^2\right]$$
$$+\kappa_2\left[\rho_1^2\left[\frac{\partial\phi_1}{\partial y}\right]^2+\left[\frac{\partial\rho_1}{\partial y}\right]^2+\rho_2^2\left[\frac{\partial\phi_2}{\partial x}\right]^2+\left[\frac{\partial\rho_2}{\partial x}\right]^2\right]. \quad (13)$$

The first term with the λ coefficient is the "Lifschitz invariant," which favors the onset of the incommensurate phase. Its form shows that the set of coordinates (ρ_1,ϕ_1) can only be modulated along x, while (ρ_2,ϕ_2) can be modulated along y. κ_1 and κ_2 have to be positive in order to stabilize the modulation near $\vec{k}_0$. Their values are related to the curvatures of the soft-mode dispersion surface along [110] and [1$\bar{1}$0]. Neglecting the coupling to macroscopic quantities, the stable state is provided at each temperature by the minimum of

$$F=\int (f_1+f_3)dx\,dy\ . \quad (14)$$

Similar to the case of incommensurate phases with a two-component order parameter,[35,36] this state is determined by nonlinear differential equations, which cannot be solved explicitly. The approximations used for the two-dimensional case are extended in a straightforward manner to the considered free-energy, because in Eqs. (11) and (13), the phases ϕ_1 and ϕ_2 as well as the coordinates x and y are involved in a decoupled way. In particular, the assumptions that ρ_1 and ρ_2 are spatially homogeneous leads for the phases ϕ_i to two sine-Gordon equations with identical coefficients:

$$\frac{d^2\phi_i}{dx_i^2}=-\frac{\beta_2}{2\kappa_1}\rho_i^2\sin[4\phi_i(x_i)] \quad (15)$$

with $x_1=x$ and $x_2=y$. In BSN, only one of these equations remains ($\rho_i\neq0$, $\rho_j=0$), and the situation with this material is therefore identical to that of a two-component order parameter which has been thoroughly investigated by various authors.[36]

As pointed out above, the results of these theoretical investigations are consistent with the standard part of the experimental data in BSN. However, they do not seem to contain any possibility of accounting for the anomalous effects such as the large thermal hysteresis at T_I.

Another type of explanation must be searched for this phenomenon and for the unusual temperature dependence of the modulation, i.e., the occurrence of a residual incommensurability below T_{II}, and the linear variation of δ in phase I which contrasts with the convex shaped variations resulting from the theory.[35]

We can note that in a few other materials, similar effects have been previously encountered. The persistence at low temperature of a nearly-commensurate phase has been observed in the transition metal dichalcogenide 1T-TaS_2.[37] The existence of a thermal hysteresis in the incommensurate phase has been recently noticed in Rb_2ZnCl_4.[38] In these two substances, the anomalous features were attributed to the influence of defects related to impurities or to a nonstoichiometry of the samples.

In BSN the crystals actually always possess a nonstoichiometry with respect to the barium and

sodium cations. Besides, even in nearly stoichiometric samples the thermal history of the crystal above 800 °C is known to influence in a significant way[39] the cation distribution in the cubic and pentagonal tunnels of the structure. Similar to the case of the above-mentioned materials, we can therefore assume that in BSN, the origin of the nonstandard effects is provoked by the local distribution related to the off-stoichiometry or off-equilibrium distribution of the alkali-alkaline earth cations in the structure. This assumption is supported by certain preliminary measurements. For instance, birefringence measurements performed on off-stoichiometry samples of different compositions shows a modified shape and magnitude of the thermal hysteresis. Also, x-ray precession photographs of differently prepared samples show that at room temperature, the residual value of δ varies between $\delta \approx 0 \pm 0.005$ and 0.02 ± 0.005.

In Rb_2ZnCl_4 the thermal hysteresis initiates some 30 °C below T_I. Simultaneously, the modulation wavelength starts varying significantly. In the framework of the existing phenomenological theories this variation is associated with a nonsinusoidal character of the modulation, i.e., the presence of discommensurations.[40] The explanation assumed[38] to account for the thermal hysteresis is based on the pinning of the discommensurations by impurities. This pinning exerts a retardation of the variations with respect to the equilibrium ones. The same type of mechanism has been considered by Nakanishi[41] to account for the transformation of the convex variations of δ in the "pure system" into a concave one in the impure one. In BSN the hysteresis starts at T_I and includes, in its range, the incommensurate phase I, in which no evidence of harmonics of the modulation has been found. The fact that δ varies significantly between T_{II} and T_I suggests that discommensurations might nevertheless exist in phase I even near T_I and that the origin of the hysteresis could be similar to that of Rb_2ZnCl_4. The absence of the higher-order satellites in the diffraction spectra would then be due to the reduction of their intensitities by a mechanism, which is unclear at present. The presence of these pinned discommensurations would also account for the departure of the modulation from a standard convex variation.

On the other hand, the behavior in BSN resembles that of doped $1T$-TaS_2 by the stabilization of a nearly commensurate phase at low temperatures and the widening of the range of the incommensurate phase I on deviating from stoichiometry. However, the simultaneous existence of a thermal hysteresis does not seem to be a marked effect in doped $1T$-TaS_2.[37]

Thus BSN displays both characteristics of $1T$-TaS_2 and Rb_2ZnCl_4 and some qualitative and quantitative differences with each of these systems. In particular, though a thermal hysteresis exists in Rb_2ZnCl_4, it is much smaller than that observed in BSN. Consequently, it is not clear whether the mechanisms invoked[38,41,42] to account for the influence of defects in the other materials will be valid for BSN. We can also note that the disappearance on cooling of the T_{II} transition resembles the suppression of a lock-in transition on cooling which has recently been described in $2H$-$TaSe_2$ (Ref. 43) and for which no interpretation has yet been put forward.

V. CONCLUSION

The behavior of BSN revealed by this study is dual. In the first place, static and dynamic features which are commonly associated to the occurrence of incommensurate phases of the displacive type have been observed: limited stability of the incommensurate phases between T_{II} and T_I, variations of the modulation wavelength in this temperature range, and driving of the transition by a soft mode. The investigation has permitted a quantitative specification of these features. The transitions at T_{II} and T_I have been assigned, respectively, as first and second order. The parameter δ characterizing the modulation has been shown to vary linearly between T_{II} and T_I.

The dynamics has only been examined in detail above T_I. The soft mode associated with T_I closely resembles that described by Dorner *et al.*[25] in gadolinium molybdate, which moves out of the overdamped regime only far above the transition. An additional similarity is the low value of the underdamped soft-mode frequency at high-temperature $\simeq 30$ cm^{-1} for $T - T_I \simeq 400$ °C in BSN and $\simeq 25$ cm^{-1} at $T - T_c \simeq 500$ °C in gadolinium molybdate. Below T_I no phonon peak could be detected, but only a wide central component with a temperature dependent intensity. This result is consistent with the previously stated failure to observe a critically varying excitation in the Raman spectra below T_I.[19] A central peak has also been observed above T_I with an intensity diverging at T_I. This peak was shown to be distinct, in the transition region, from the contribution of the

overdamped phonon. Its width was not resolved.

We have related satisfactorily the onsets of the incommensurate phase, the improper character of the ferroelastic properties of BSN, and the approximate space symmetry of the room-temperature phase through the identified peculiarities of the four-component order parameter associated to the T_I transition. On the other hand, the occurrence of unusual phenomena has been pointed out. These comprise the persistence of a residual incommensurability below T_{II} and a qualitative difference between the heating and cooling measurements.

We have shown that this behavior was not likely to be accounted for by the four-component order-parameter Landau expansion since this expansion is expected to determine the same sequence of phenomena, i.e., a convex variation of the modulation δ and the existence of a lock-in at T_{II}, as in the well-known case of a two-dimensional order parameter.

Similar to the case of recently investigated substances, the anomalous behavior has been suggested to be due to the influence of defects related to the off-stoichiometric distribution of cations in the structure. The significant role of defects in the behavior of BSN would also be consistent with the observation of a central peak even far above the transition T_I. This role has yet to be established more specifically by a detailed experimental study of the behavior as a function of stoichiometry. Preliminary measurements in other members of the tungsten-bronze family show that BSN does not display an isolated behavior. We have observed similar incommensurate phases in several compounds. They seem to possess the same order-parameter characteristics as that of BSN. These results suggest that the properties presented here belong to an entire structural family with incommensurate phases for which the oxygen octahedral structure plays the central role.

ACKNOWLEDGMENTS

We express our thanks to Dr. B. Dorner for helpful advice and discussions. We are grateful to P. Florès and Mr. Serve for the expert advice they provided for using the experimental setup. We have benefitted from the helpful assistance of C. Lamborelle during the experiment. We are grateful to A. M. Pougnet who performed the DTA measurements, and to R. Mellet who measured the composition of the samples. Discussions with G. Errandonéa have clarified the problems of the central peak and the phonon damping. We thank Dr. R. Currat for useful comments on the manuscript.

---

*Present address: Laboratoire Léon Brillouin, CEN-Saclay BP2, 91190 Gif sur Yvette, France.

[1] *Landolt-Bornstein: Ferroelectric and Antiferroelectric Substances* (Springer, New York, 1969).
[2] A. Magneli, Ark. Kem. 1, 213 (1960).
[3] F. Jona and G. Shirane, Ferroelectric Materials (Pergamon, New York, 1962).
[4] E. A. Giess, B. A. Scott, G. Burns, D. F. O'Kane, and A. Segmüller, J. Am. Ceram, Soc. 52, 276 (1969).
[5] L. G. Van Uitert, J. J. Rubin, and W. A. Bonner, I.E.E.E. Quantum Electron. 4, 622 (1968).
[6] S. Singh, D. A. Draegert, and J. E. Geusic, Phys. Rev. B 2, 2709 (1970).
[7] J. Schneck, J. Primot, J. Ravez, and R. Von der Mühl, Solid State Commun. 21, 57 (1977).
[8] J. Schneck and D. Paquet, Ferroelectrics 21, 577 (1978).
[9] J. Sapriel and A. Boudou, Ferroelectrics 21, 323 (1978).
[10] J. Schneck, B. Joukoff, and R. Mellet, Ferroelectrics 26, 775 (1980).
[11] J. Schneck, J. C. Tolédano, B. Joukoff, F. Denoyer, and C. Joffrin, Ferroelectrics 26, 661 (1980).
[12] J. Schneck and F. Denoyer, Phys. Rev. B 23, 383 (1981).
[13] T. Yamada, H. Iwasaki, and N. Niizeki, J. Appl. Phys. 41, 4141 (1970).
[14] J. C. Tolédano, Phys. Rev. B 12, 943 (1975).
[15] J. C. Tolédano and M. Busch, J. Phys. (Paris) Lett. 36, L41 (1975); J. C. Tolédano, M. Busch, and J. Schneck, Ferroelectrics 13, 327 (1976).
[16] P. B. Jamieson, S. C. Abrahams, and J. L. Bernstein, J. Chem. Phys. 50, 4352 (1969).
[17] L. C. Bobb, I. Lefkowitz, and L. Muldawer, J. Appl. Crystallogr. 2, 189 (1969).
[18] J. Burgeat and J. C. Tolédano, Solid State Commun. 20, 281 (1976).
[19] A. Boudou and J. Sapriel, Phys. Rev. B 21, 61 (1980).
[20] W. A. Bonner, J. R. Carruthers, and H. M. O'Bryan, Mater. Res. Bull. 5, 243 (1970).
[21] C. F. Majkrzak, J. D. Axe, and A. D. Bruce, Phys. Rev. B 21, 5278 (1980).
[22] K. Gesi and M. Iizumi, J. Phys. Soc. Jpn. 46, 697 (1979).

[23]M. J. Cooper and R. Nathans, Acta. Crystallogr. 23, 357 (1967).
[24]A. D. Bruce and R. A. Cowley, Adv. Phys. 29, 219 (1980).
[25]B. Dorner, J. D. Axe, and G. Shirane, Phys. Rev. B 6, 1950 (1972).
[26]P. M. DeWolff, Acta Crystallogr. A30, 777 (1974).
[27]G. C. Dubbeldam and P. M. DeWolff, Acta Crystallogr. B25, 2665 (1969).
[28]S. C. Abrahams, P. B. Jamieson, and J. L. Bernstein, J. Chem. Phys. 54, 2555 (1971).
[29]Preliminary assignment to *Bmm*2 (Ref. 11) had been performed in a multidomain sample which provided a mixing of (*hkl*) and (*khl*) reflections.
[30]J. C. Tolédano and P. Tolédano, Phys. Rev. B 21, 3380 (1980).
[31]D. Mukamel and S. Krinsky, Phys. Rev. B 13, 5078 (1976).
[32]D. E. Cox, S. M. Shapiro, R. A. Cowley, M. Eibschutz, and H. J. Guggenhein, Phys. Rev. B 19, 5754 (1979).
[33]R. Pynn and J. D. Axe, J. Phys. C. 9, L199 (1976).
[34]J. Schneck and P. Bastie (unpublished).
[35]R. A. Cowley, Adv. Phys. 29, 1 (1980).
[36]A. P. Levanyuk and D. G. Sannikov, Fiz. Tverd. Tela (Leningrad) 18, 423 (1976) [Sov. Phys.—Solid State 18, 423 (1976)].
[37]F. J. DiSalvo, J. A. Wilson, B. G. Bagley, and J. V. Waszczack, Phys. Rev. B 12, 2220 (1975).
[38]K. Hamano, Y. Ikeda, T. Fujimoto, K. Ema, and S. Hirotsu, J. Phys. Soc. Jpn. 49, 2278 (1980).
[39]G. Burns and B. E. Scott, Phys. Lett. 28A, 776 (1969).
[40]W. L. McMillan, Phys. Rev. B 14, 1496 (1976); Y. Ishibashi, Ferroelectrics 20, 103 (1978).
[41]K. Nakanishi, J. Phys. Soc. Jpn. 46, 1434 (1979).
[42]L. J. Sham and B. R. Patton, Phys. Rev. B 13, 3151 (1976).
[43]R. M. Fleming, D. E. Moncton, D. B. McWhan, and F. J. DiSalvo, Phys. Rev. Lett. 45, 576 (1980).